

Dislocation nucleation during nanoindentation of aluminum

R. J. Wagner,^{a)} L. Ma, F. Tavazza, and L. E. Levine

Metallurgy Division, National Institute of Standards and Technology, Gaithersburg, Maryland 20899, USA

(Received 4 March 2008; accepted 5 October 2008; published online 8 December 2008)

Through multiscale simulations, we explore the influence of both smooth and atomically rough indenter tips on the nucleation of dislocations during nanoindentation of single-crystal aluminum. We model the long-range strain with finite element analysis using anisotropic linear elasticity. We then model a region near the indenter atomistically and perform molecular dynamics with an embedded atom method interatomic potential. We find that smooth indenters nucleate dislocations below the surface but rough indenters can nucleate dislocations both at the surface and below. Increasing temperature from 0 to 300 K creates prenucleation defects in the region of high stress and decreases the critical depth. [DOI: [10.1063/1.3021305](https://doi.org/10.1063/1.3021305)]

I. INTRODUCTION

Nanoindentation is the most widely used experimental method for exploring plastic mechanical properties of materials at the nanoscale.¹⁻³ During nanoindentation, a probe, typically with a diamond tip, is pressed into a sample material and then retracted. Measuring the applied force versus displacement into the sample yields information about the material properties.

The force versus displacement profile for nanoindentation into aluminum typically exhibits two features during the early stages of loading. The sample initially responds elastically with the force increasing rapidly until some critical point is reached when the profile exhibits a discontinuity as irreversible deformation occurs, usually through fracture of an oxide layer or dislocation-mediated plasticity.⁴

Ideally, experiments are conducted with indenters that perfectly match a prescribed geometry. For example, a Berkovich indenter is defined to be a three-sided pyramid with the faces tilted 65° off axis.⁵ Real indenters diverge from these idealized geometries due to material limitations, machining defects, or mechanical wear. At scales below 100 nm, a Berkovich indenter is often approximated by a sphere rather than a pyramid, although atomic force microscopy (Fig. 1) shows that the actual shape can be very complex. These mesoscale shape changes have a pronounced effect on the stress distribution in the sample during nanoindentation.^{6,7} Furthermore, at the even finer scale of atoms, an indenter exhibits unavoidable roughness due to steps resulting from termination of the bulk crystal structure.

Dislocation nucleation is generally assumed to occur below the sample surface at the location of highest resolved shear stress.⁴ However, it has been observed experimentally that atomic steps on the surface of gold samples can significantly affect the measured critical stress where plastic deformation occurs,⁸ suggestive of surface nucleation in that case. The question of surface versus bulk nucleation cannot be answered through postmortem studies of indented surfaces since the elastic energy stored in the sample during the elastic loading phase will drive significant dislocation multiplication after the nucleation threshold is reached. Instead, mul-

tiscale atomistic simulations are required where the important long-range elastic strain fields are properly taken into account. The possibility that atomic steps on the sample surface can affect dislocation nucleation also raises an interesting general question about nanoindentation experiments; namely, how does the unavoidable atomic-scale roughness of a *nanoindenter tip* affect the measurement?

Several previous studies have explored aspects of dislocation nucleation during nanoindentation of face-centered cubic metals. Gouldstone *et al.*⁴ conducted nanoindentation experiments into single-crystal Al and detected displacement bursts associated with the formation of dislocations. Li *et al.*⁹ and Van Vliet *et al.*¹⁰ performed molecular dynamics (MD) simulations of spherical indentation into $\langle 111 \rangle$ Al, finding nucleation on $\{111\}\langle 110 \rangle$ slip systems from small, perfectly smooth indenters. Tsuru and Shibutani¹¹ performed similar simulations to find the magnitude and location of shear stress necessary to nucleate dislocations. They examined variation with larger indenter radii but only at zero temperature and without indenter roughness. Gouldstone *et al.*¹² reported defect nucleation in a bubble raft model with surface roughness producing defects in the asperities.

In the present study we perform multiscale simulations to examine the nucleation of dislocations in a single-crystal Al sample and explore the role of unavoidable indenter roughness. This differs from the previous work in our approach to create a realistic long-range elastic strain field, in

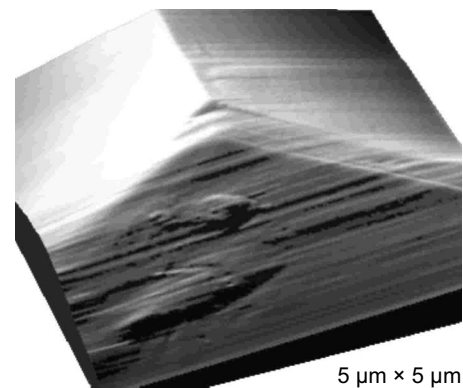


FIG. 1. Atomic force micrograph of a pyramidal indenter showing rounding and roughness at small scales.

^{a)}Electronic mail: wagnerr@umich.edu.

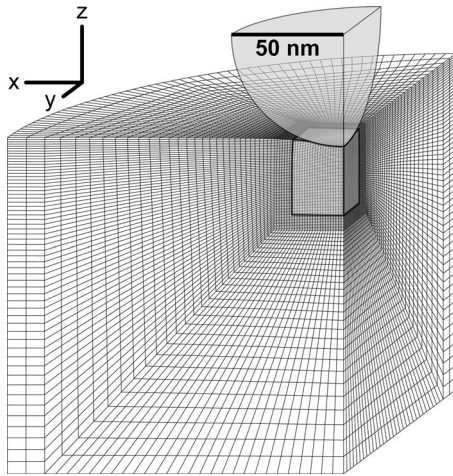


FIG. 2. Cutaway view of finite element mesh during indentation to 5 nm showing the atomistic region (outlined) within the fine region.

our attention to the effects of indenter tip roughness, and in our comparison of zero temperature and room temperature conditions.

II. METHODS

The critical dislocation nucleation event described above is driven by the large elastic strain energy stored during the elastic loading of the specimen by the indenter. In order to connect the dislocation nucleation to the applied load and the indentation depth, it is therefore necessary to accurately model the long-range elastic strain fields in the sample using a continuum approach such as finite element analysis (FEA). The dislocation nucleation process is then modeled atomistically. Since the focus of this paper is dislocation *nucleation* and not the subsequent evolution of the resulting dislocation structures, it is not necessary to implement bidirectional handshaking between continuum and atomistic regions. We use the continuum solution to define the boundary conditions and initial atom positions for the subsequent atomistic simulations.

We begin the simulation with FEA of the elastic interaction between the indenter and the specimen using the commercial code ABAQUS.¹³ At this stage, the indenter is modeled as a rigid frictionless sphere with a radius of 50 nm. The specimen is modeled as a $\langle 111 \rangle$ -oriented single-crystal Al using orthotropic (elastic) deformation with elastic constants set to match the atomistic model described below at zero temperature. To remove boundary effects from the vicinity of the indenter, the specimen is modeled as a wide cylinder, 300 nm in diameter and 150 nm tall, with the bottom fixed and the top pressed upon by the indenter.

To simplify the connection to an atomistic model we use a fine mesh in a $45.8 \times 47.6 \times 29.4$ nm³ region directly below the indenter as shown in Fig. 2. Each element contains 48 Al atoms and is aligned with its nodes coincident with single-crystal Al atom positions as detailed in Ref. 7. The element size then increases linearly with distance away from the fine region.

From the FEA indentation simulation we obtain the elastic displacement of each node due to penetration of the in-

denter into the sample. We repeat the calculations for indentations ranging from 0.0 to 5.0 nm at 0.5 nm intervals and interpolate to produce displacement fields at 0.1 nm intervals. We then prepare a MD simulation by interpolating atom positions from node positions in the fine region. This atomistic region contains 3 920 555 atoms and fully encompasses the area of contact with the indenter. It also incorporates the correct long-range elastic displacement field while drastically reducing the computational cost of the simulation compared to a fully atomistic approach.

The energy and forces for dynamics are calculated with an embedded atom method (EAM) potential¹⁴ for aluminum.¹⁵ This potential is based on both experimental lattice properties and *ab initio* energies for various crystal structures, vacancies, and stacking faults. We hold fixed the atoms within the EAM cutoff distance (0.63 nm) of the side and bottom surfaces of the atomistic region. The remaining atoms are allowed to move according to MD with a velocity Verlet algorithm and a time step of 1 fs. We apply a velocity scaling thermostat¹⁶ to set the system temperature T to either 0 or 300 K.

Our method derives the initial atom positions from the FEA simulation and maintains the boundary atoms at fixed positions during the MD simulation. We do not feed back forces from the atomistic region into the surrounding FEA region since such forces will be negligible until after the moment of nucleation at which our simulation ends. A study of the plastic evolution after dislocation nucleation would require such feedback and is beyond the scope of this paper. Likewise, we ignore thermal coupling to the FEA region, which would produce less significant improvement in realism compared to that already obtained over conventional rigid or periodic boundary conditions.

During the MD simulation, the top surface of the atomistic region is constrained by one of two indenter models. The first model is a smooth indenter represented as a single superatom with a 50 nm radius. The second model is an atomically rough indenter formed by carving a spherical block of carbon atoms (0.25 nm radius) from a perfect diamond lattice (0.356 nm lattice constant) with a $\langle 111 \rangle$ axis along the indentation direction. In both cases the energy between the indenter atoms and the sample atoms is described by $(R-r)^3 \times 3.0$ eV/Å³ for $r < R$ where R is the indenter atom radius and r is the indenter-sample atom separation.¹⁷

Defects within the evolving sample are visualized by classification of the atoms according to centrosymmetry, with higher asymmetry indicating stacking faults, partial dislocations, and surfaces.¹⁷ The critical load for plastic deformation is determined by repeating the MD simulation with the FEA elastic displacement field for each indentation depth. The smallest depth that produces dislocation nucleation during 40 000 time steps (40 ps) is taken as the critical depth. In simulations of subcritical indentations at 0 K, this period is sufficient for the atomic forces to relax without dislocation nucleation. In simulations at 300 K nucleation is a stochastic process and this period gives an upper bound on the critical depth. Since our interest is only the initial stages of dislocation and growth, the simulations are terminated before dislocations reach the boundary of the atomistic region.

TABLE I. Conditions for dislocation nucleation.

Indenter	T (K)	Depth (nm)	Load (nN)	τ_{\max} (GPa)	τ_{nuc} (GPa)	τ_{res} (GPa)
Smooth	0	4.4	8600	5.7	5.2	4.3
Smooth	300	3.1	5000	4.7	4.2	4.1
Rough	300	3.3	5500	4.9	4.6	3.8
Rough	0	4.5	8900	5.8	3.7	3.6

III. RESULTS AND DISCUSSION

Table I summarizes the conditions for dislocation nucleation with each indenter at each temperature. Three characteristic shear stresses are extracted from the FEA simulation: τ_{\max} is the maximum shear stress anywhere in the specimen, τ_{nuc} is the shear stress at the actual nucleation site, and τ_{res} is the highest resolved $\{111\}\langle 110 \rangle$ shear stress at that site. For comparison, Al modeled with this EAM potential has a theoretical shear strength of about 4.1 GPa (estimated by $G/2\pi$ where G is the shear modulus). Figure 3 shows the defect structure evolution during dislocation nucleation.

For the smooth indenter at 0 K, the first leading partial dislocation nucleates after indentation to 4.4 nm and appears 9.8 nm below the original surface and 8.5 nm off the indentation axis in the area of highest resolved $\{111\}\langle 110 \rangle$ shear stress. A stacking fault extends behind the leading partial until a trailing partial nucleates and the stacking-fault ribbon collapses. The energetically unfavorable dynamic stacking faults persist up to sizes of 20 nm because the near-zero temperature starves them of the activation energy needed to

form trailing partial dislocations. Meanwhile, a second and third group of dislocations nucleate at symmetric locations on sister $\{111\}$ planes.

To examine the effect of temperature on indentation, we repeat the simulations with the smooth indenter at 300 K. At this temperature, “hot-spot” defects appear due to the asymmetry produced by thermal vibrations.¹⁸ The magnitude of asymmetry and the density of these transitory defects are enhanced in the regions of highest local shear stress, particularly in a volume 20 nm wide at a depth of 5–15 nm below the indenter. This volume includes the three symmetric locations of maximum resolved shear stress for the primary slip systems. These defects decrease the static load required for dislocation nucleation, reducing the critical depth to 3.1 nm. The first dislocation nucleates 9.6 nm below the surface and 5.4 nm off axis. Loops grow along $\{111\}$ planes from that spot and form closely spaced pairs of partial dislocations rather than maintaining large stacking faults.

It is interesting to note that the previous modeling work by Zuo *et al.*¹⁸ on hot-spot defects was conducted with uniform stress fields. In the present work, the indenter stress field varies smoothly through the specimen, allowing us to examine the dynamics of how these fluctuations interact with that field. We find that although the transitory defects occur everywhere within the region of high shear stress under the indenter tip, they persist longer (and grow larger) in the three symmetric locations corresponding to maximum resolved $\{111\}\langle 110 \rangle$ shear stress. We can therefore interpret these defects as subcritical incipient dislocations.

Having examined dislocation nucleation from the smooth indenter at both temperatures, we turn to simulations with the atomically rough indenter. At 300 K it produces the same cloud of hot spots as the smooth one, but it also generates numerous surface defects associated with its atomic ledges. The local stresses in the vicinity of the ledges are high enough to produce tiny 1 nm long dislocation loops at the point of contact, but the stress field below these loops is insufficient for them to grow. These nascent dislocations are visible in Fig. 3 as small protrusions from the surface near the center of the indenter. Meanwhile the thermal fluctuations in the bulk region below the indenter activate the nucleation of a separate dislocation loop 9.2 nm below the surface and 5.7 nm off axis, near the expected location with highest resolved $\{111\}\langle 110 \rangle$ shear stress. This second loop grows and spawns more dislocation loops in a process identical to that for the smooth indenter. The critical indentation depth of 3.3 nm is comparable to that for the smooth indenter at this temperature.

As we have just seen, the local stress fields produced by

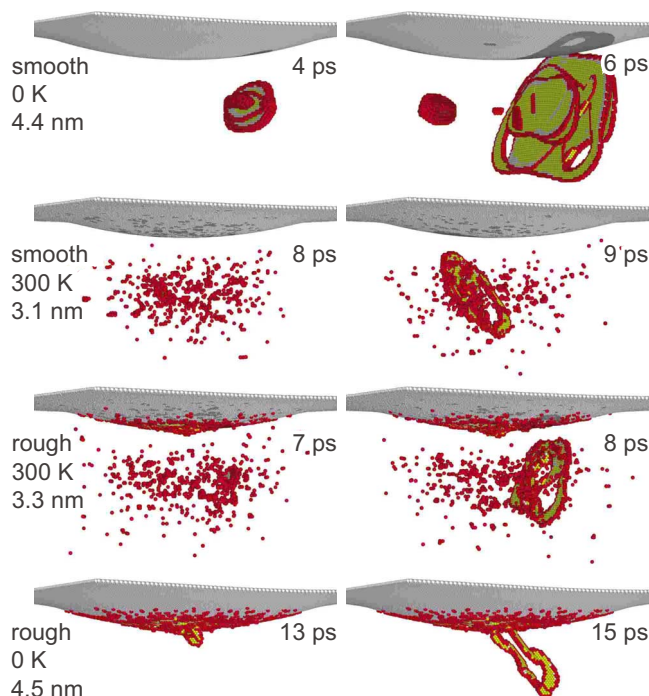


FIG. 3. (Color online) Defect structures at critical depths with atoms colored by centrosymmetry: surface (gray), partial dislocation (red), and stacking fault (yellow). Labels indicate indenter type, temperature, indentation depth, and time.

atomic ledges on the rough indenter are large enough to nucleate dislocations near the surface but the nearby stresses are insufficient to drive further growth. Instead, bulk nucleation promoted by thermal fluctuations dominates the plasticity. If we lower the temperature to suppress those fluctuations then we could shift the balance between the competing dislocation nucleation and growth mechanisms. A simulation with the rough indenter at 0 K shows no hot-spot defects beneath the indenter, leaving only the surface defects as possible heterogeneous nucleation sites. As with the 300 K simulation, atomic roughness on the indenter causes dislocations to nucleate near the point of contact. Now, however, the nearby stresses are much higher due to the increased indentation depth of 4.5 nm, and a surface loop is able to grow. Thus the dislocation nucleation mechanism in this case operates at the surface rather than in the bulk. As in other cases where the dislocation nucleation mechanism involves heterogeneities, the barrier to nucleating the trailing partial is low and the stacking fault ribbon is narrow. Our observation of surface dislocation nucleation from a rough indenter parallels bubble raft models in which a smooth indenter impacting a rough surface produces plasticity in atomic scale asperities.¹²

The stresses extracted from the FEA simulations (Table I) are fully consistent with the observed nucleation behavior. The maximum stress resolved on a $\{111\}$ plane in a $\langle 110 \rangle$ direction τ_{res} was 4.3 GPa for the smooth indenter at 0 K, in good agreement with the theoretical shear stress of 4.1 GPa. Raising the temperature decreases the shear stress necessary for bulk dislocation nucleation as seen from the results for both indenters at 300 K. The rough indenter at 0 K has the lowest value for τ_{res} because that nucleation event was driven by surface stress concentration at an atomic ledge whereas the other critical nucleation events occurred in the bulk. This value matches the critical resolved shear stress σ_c necessary for incipient dislocation growth. For the observed dislocation loops with diameter $L \approx 1$ nm and Burgers vector b , the Frank–Read critical stress for edge dislocations is $\sigma_c = Gb/2L = 3.8$ GPa, in good agreement with the near-surface stress.

Across the full set of conditions studied, the critical depth for dislocation nucleation ranged from 3.1 to 4.5 nm, comparable to critical depths of less than 10 nm measured experimentally.⁴ An important observation is that the simulations at 300 K nucleate dislocations about 1.2 nm earlier than at 0 K, corresponding to a 40% decrease in the applied load. This difference in the critical load is mostly independent of the indenter roughness and is an important consideration when comparing zero-temperature models of nanoindentation to experimental results.

IV. CONCLUSIONS

Our multiscale simulation method combines realistic long-range elasticity with local atomistic plasticity, allowing us to directly relate the applied load to the dislocation nucleation behavior. At both 0 and 300 K, the smooth indenter caused the first dislocations to nucleate below the sample surface on $\{111\}$ planes at positions of high resolved shear stress. Thermal vibrations at 300 K decreased the energy

barrier to bulk dislocation nucleation, resulting in a reduced critical depth and critical load. Introducing atomic roughness on the indenter tip produced surface defects near the ledge positions, thus locally reducing the energy barrier for surface nucleation of dislocations. At both temperatures examined the first dislocations nucleated heterogeneously from these surface defects. At 300 K the stresses near the surface were too low to drive growth of those dislocations before bulk nucleation and growth occurred below the surface. However, at 0 K the thermal fluctuations were suppressed and increasing the indenter load applied sufficient stress to drive those dislocations into the bulk.

Thus, we observe that the underlying dislocation nucleation mechanism for atomically rough indenters is temperature dependent, with surface nucleation favored at lower temperatures. This is in marked contrast with the usual assumption that bulk dislocation nucleation always dominates during nanoindentation. Furthermore, real indenter tips are expected to be rougher than the minimally rough indenter explored here and the corresponding surface stresses would be significantly larger. Future work will examine how the much rougher nanoscale shapes of real indenters alter the onset and measurement of plasticity.

ACKNOWLEDGMENTS

This study utilized the high-performance computational capabilities of the Biowulf Linux cluster at the National Institutes of Health, Bethesda, Md. (<http://biowulf.nih.gov>).

Certain commercial software, equipment, instruments, or materials are identified in this paper to specify adequately the experimental and computational procedure. Such identification does not imply recommendation or endorsement by the National Institute of Standards and Technology, nor does it imply that the materials or equipment identified are necessarily the best available for the purpose.

¹M. F. Doerner and W. D. Nix, *J. Mater. Res.* **1**, 601 (1986).

²A. C. Fisher-Cripps, *Nanoindentation* (Springer-Verlag, New York, 2002).

³W. C. Oliver and G. M. Pharr, *J. Mater. Res.* **7**, 1564 (1992).

⁴A. Gouldstone, H.-J. Koh, K.-Y. Zeng, A. E. Giannakopoulos, and S. Suresh, *Acta Mater.* **48**, 2277 (2000).

⁵E. S. Berkovich, *Ind. Diamond Rev.* **11**, 129 (1951).

⁶G. Constantinides, E. C. C. M. Silva, G. S. Blackman, and K. J. Van Vliet, *Nanotechnology* **18**, 305503 (2007).

⁷L. Ma and L. E. Levine, *J. Mater. Res.* **22**, 1656 (2007).

⁸J. D. Kiely, R. Q. Hwang, and J. E. Houston, *Phys. Rev. Lett.* **81**, 4424 (1998).

⁹J. Li, K. J. Van Vliet, T. Zhu, S. Yip, and S. Suresh, *Nature (London)* **418**, 307 (2002).

¹⁰K. J. Van Vliet, J. Li, T. Zhu, S. Yip, and S. Suresh, *Phys. Rev. B* **67**, 104105 (2003).

¹¹T. Tsuru and Y. Shibutani, *Modell. Simul. Mater. Sci. Eng.* **14**, S55 (2006).

¹²A. Gouldstone, K. J. Van Vliet, and S. Suresh, *Nature (London)* **411**, 656 (2001).

¹³Abaqus/Standard, *Theory and User's Manual, Version 6.6* (ABAQUS, Providence, RI, 2006).

¹⁴M. S. Daw and M. I. Baskes, *Phys. Rev. B* **29**, 6443 (1984).

¹⁵Y. Mishin, D. Farkas, M. J. Mehl, and D. A. Papaconstantopoulos, *Phys. Rev. B* **59**, 3393 (1999).

¹⁶W. C. Swope and H. C. Andersen, *J. Chem. Phys.* **76**, 637 (1982).

¹⁷C. L. Kelchner, S. J. Plimpton, and J. C. Hamilton, *Phys. Rev. B* **58**, 11085 (1998).

¹⁸L. Zuo, A. H. W. Ngan, and G. P. Zheng, *Phys. Rev. Lett.* **94**, 095501 (2005).